Published in final edited form as:
J Immunol. 2014 August 15; 193(4): 1942–1953. doi:10.4049/jimmunol.1301941.

Myeloid-Derived Suppressor Cells Are Involved in Lysosomal Acid Lipase Deficiency-Induced Endothelial Cell Dysfunctions

Ting Zhao[*], **Xinchun Ding**[*], **Hong Du**[*,†], and **Cong Yan**[*,†,‡]

[*]Department of Pathology and Laboratory Medicine, Indiana University School of Medicine, Indianapolis, IN 46202

[†]IU Simon Cancer Center, Indiana University School of Medicine, Indianapolis, IN 46202

[‡]Center for Immunobiology, Indiana University School of Medicine, Indianapolis, IN 46202

Abstract

The underlying mechanisms that lysosomal acid lipase (LAL) deficiency causes infiltration of myeloid-derived suppressor cells (MDSCs) in multiple organs and subsequent inflammation remain incompletely understood. Endothelial cells (ECs), lining the inner layer of blood vessels, constitute barriers regulating leukocytes transmigration to the site of inflammation. Therefore, we hypothesized that ECs are dysfunctional in LAL-deficient ($lal^{-/-}$) mice. We found that $Ly6G^+$ cells transmigrated more efficiently across $lal^{-/-}$ ECs than wild-type ($lal^{+/+}$) ECs, which was associated with increased level of platelet endothelial cell adhesion molecule-1 (PECAM-1) and monocyte chemoattractant protein-1 (MCP-1) in $lal^{-/-}$ ECs. In addition, $lal^{-/-}$ECs showed enhanced migration and proliferation, decreased apoptosis, but impaired tube formation and angiogenesis. $lal^{-/-}$ ECs also suppressed T cell proliferation *in vitro*. Interestingly, $lal^{-/-}$ $Ly6G^+$ cells promoted *in vivo* angiogenesis (including a tumor model), EC tube formation and proliferation. Finally, the mammalian target of rapamycin (mTOR) pathway was activated in $lal^{-/-}$ ECs, and inhibition of mTOR reversed EC dysfunctions, including decreasing $Ly6G^+$ cell transmigration, delaying migration, and relieving suppression of T cell proliferation, which was mediated by decreasing production of reactive oxygen species (ROS). Our results indicate that LAL regulates EC functions through interaction with MDSCs and modulation of the mTOR pathway, which may provide a mechanistic basis for targeting MDSCs or mTOR to rejuvenate EC functions in LAL-deficiency related diseases.

Introduction

Lysosomal acid lipase (LAL) hydrolyzes cholesteryl esters and triglycerides in the lysosome of cells to generate free fatty acids and cholesterol. LAL deficiency has been reported to result in pulmonary inflammation, which is associated with neutrophil infiltration, increases of foamy macrophages and alternation of proinflammatory cytokines/chemokines (1, 2).

Address correspondence to: Dr. Cong Yan, Department of Pathology and Laboratory Medicine, Indiana University School of Medicine, 975 W Walnut Street, IB424G, Indianapolis, IN 46202. coyan@iupui.edu; Tel: 317-278-6005; or Dr. Hong Du, Department of Pathology and Laboratory Medicine, Indiana University School of Medicine, 975 W Walnut Street, IB424E, Indianapolis, IN 46202. hongdu@iupui.edu; Tel: 317-274-6535..

Disclosures The authors have no financial conflicts of interest.

Endothelial cells (ECs), which play a crucial role in regulating blood flow, controlling vessel-wall permeability, and quiescing circulating leukocytes, are both active participants and regulators of inflammatory processes at a site of inflammation (3). Failure of ECs to adequately perform their functions constitutes endothelial cell dysfunction. In LAL-deficient ($lal^{-/-}$) mice, whether LAL deficiency-induced myeloid lineage cell infiltration is related to EC dysfunctions has not been studied yet.

Myeloid-derived suppressor cells (MDSCs), characterized by the co-expression of myeloid-cell lineage differentiation markers Ly6G and CD11b, are a heterogeneous population of immature myeloid cells, whose accumulation is associated with multiple pathological conditions (4-6). Recent studies addressed the roles of tumor-associated MDSCs in the interplay between immune suppression and angiogenesis, showing that angiogenic factors produced by MDSCs facilitated EC angiogenic functions (7-9). We previously reported that the neutral lipid metabolic pathway controlled by LAL plays a critical role in the development and homeostasis of MDSCs, and have demonstrated that LAL deficiency led to the infiltration and accumulation of MDSCs in various tissues of the mice, such as the lung, spleen, thymus, liver and small intestine (10-12). $lal^{-/-}$ MDSCs possess both immune suppressive function and tumor stimulatory function (13, 14). However, little is known about whether and how MDSCs influence EC functions during LAL deficiency.

The mammalian target of rapamycin (mTOR) is a serine/threonine protein kinase that regulates cell growth, proliferation, motility, survival, protein synthesis, and transcription in response to growth factors and mitogens (15). In ECs, mTOR acts as a regulatory kinase, playing an important role in EC survival, migration, and proliferation (16). We have recently demonstrated that in $lal^{-/-}$ mice, the mTOR pathway was over-activated in bone marrow-derived MDSCs (17). However, it is unknown whether the mTOR pathway is overly activated in $lal^{-/-}$ ECs, and whether over-activation of this pathway is involved in EC dysfunctions.

In the present study, EC functions in $lal^{-/-}$ mice, including transendothelial migration for MDSCs and T cells, angiogenesis, and proliferation were determined. The ability of ECs in regulating T cell proliferation and function was studied as well. Furthermore, the effects of MDSCs on ECs were evaluated, focusing on MDSC transendothelial migration, EC angiogenesis and proliferation. Finally, the mTOR pathway was investigated in $lal^{-/-}$ ECs. Our study demonstrates for the first time that LAL deficiency results in EC dysfunctions through interaction with MDSCs and over-activation of the mTOR pathway. Overproduction of reactive oxygen species (ROS) is one of mediators involved in $lal^{-/-}$ EC dysfunctions. These findings provide a mechanistic insight into LAL in controlling EC functions.

Materials and Methods

Animals

All scientific protocols involving the use of animals have been approved by the Institutional Animal Care and Use Committee of Indiana University School of Medicine and followed guidelines established by the Panel on Euthanasia of the American Veterinary Medical

Association. Animals were housed under Institutional Animal Care and Use Committee-approved conditions in a secured animal facility at Indiana University School of Medicine.

Isolation and in vitro culture of pulmonary ECs

ECs were isolated from lungs and cultured *in vitro*, based on published protocols with some minor modifications (18, 19). Briefly, the mouse was anesthetized and 5 mL cold PBS was injected via the right ventricle to flush the blood out. One milliliter of collagenase A (2 mg/mL, Roche, Indianapolis, IN, USA) was infused into the lung through the trachea. The lung was removed and then incubated with 10 mL of collagenase A at 37°C for 30 min. After the incubation, PBS was added to the tube, and the tube was vigorously shaken to dissolve the lung. The resulting cell suspension was filtered through a 40 μm strainer and centrifuged for 5 minutes at 1,500 rpm. After removal of the supernatant, the cell pellet was subjected to magnetic bead sorting using anti-CD31 microbeads (Miltenyi Biotec., Auburn, CA, USA) according to the manufacturer's protocol. The resulting cells were plated onto gelatin (Sigma-Aldrich, St. Louis, MO, USA)-coated six-well plates and maintained in DMEM (Gibco, Grand Island, NY, USA) supplemented with endothelial cell growth supplement, heparin, L-Glutamine (Sigma-Aldrich), fetal bovine serum (FBS), and Antibiotic-Antimycotic (Gibco).

Isolation of bone marrow-derived MDSCs

MDSCs were isolated as we previously described (17, 20). Briefly, bone marrow cells were isolated from the femurs and tibias of wild-type ($lal^{+/+}$) and $lal^{-/-}$ mice. Cells were first incubated with biotin-conjugated anti-Ly6G antibody (Miltenyi Biotec.) at 4°C for 15 min. After washed with PBS, cells were incubated with anti-biotin microbeads (Miltenyi Biotec.) at 4°C for another 15 min. Subsequently, cells were subjected to magnetic bead sorting according to the manufacturer's instructions (Miltenyi Biotec.). The resulting cells were seeded into 96-well plates for further studies.

Isolation of bone marrow-derived macrophages

Macrophages were isolated based on a published protocol (21). Briefly, bone marrow cells were harvested from $lal^{+/+}$ and $lal^{-/-}$ mice. Cells were then cultured in DMEM/F12 medium (Gibco) supplemented with 10% FBS and 50 ng/mL recombinant M-CSF (R&D, Minneapolis, MN, USA). After 7 days' culture, unattached cells were removed, and more than 95% of remaining adherent cells were positive for F4/80 and CD11b by flow cytometry analysis.

Transwell assay

Transwell assay was used to determine MDSC transendothelial migration. ECs were collected by Accutase (Sigma-Aldrich) digestion. Around 5×10^4 cells in 250 μL media were added to the upper chamber of 24-well 6.5-μm-pore Transwell plates (Corning, Corning, NY, USA), while 500 μL media was placed in the lower chamber. Cells were incubated at 37°C, 5% CO_2 for 48 h to form an EC monolayer. Then the supernatant was removed, and CellTracker™ Green 5-Chloromethylfluorescein Diacetate (CMFDA) (Invitrogen, Grand Island, NY, USA)-labeled MDSCs (1×10^4 cells in 250 μL media) were added to the upper

well. The media in the lower chamber was replaced with the same media as the upper chamber. After 6 h, transendothelial migration of MDSCs was determined by counting their numbers in the lower chamber under 5 random microscopic fields. For the neutralization study, ECs were pretreated with 10 μg/mL neutralizing antibody against PECAM-1, MCP-1, IL-6, TNF-α or control IgG for 1h.

Tube formation assay

The *in vitro* angiogenic activity of ECs was determined by matrigel tube formation assay as previously described (22). Briefly, ECs were seeded at a density of 5×10^4 cells/well in 48-well plates precoated with 150 μL/well growth factor-reduced matrigel (BD Biosciences, San Jose, CA, USA). After 6 h of incubation, tube formation was observed with an inverted microscope with image capture system (Nikon, Melville, NY, USA). Tube formation was defined as a tube-like structure exhibiting a length four times its width (23). To detect the effect of MDSCs on EC tube formation, MDSCs and ECs were co-cultured overnight. Images of tube morphology were taken in 5 random microscopic fields per sample at × 40 magnification, and the cumulative tube lengths were measured by Image-Pro Plus software (Media Cybernetics, Rockville, MD, USA).

In vitro wound healing assay

In vitro wound healing assay was performed to analyze EC migration as previously described (24). Briefly, ECs were seeded at a density of 1.5×10^5 cells/well into a 24-well plate and incubated overnight to form a confluent monolayer. Scratch was created by scraping the cell monolayer in a straight line with a p200 pipet tip. After washing 3 times with PBS, the medium was changed with DMEM containing 10% FBS and 5 μg/mL mitomycin C (Sigma-Aldrich), and ECs were kept on culture at 37°C, 5% CO_2. Images were taken at 0 and 15 h after creating the scratch. Migration was estimated by measuring the distances from one side of scratch to the other side using Image Pro-Plus software (Media Cybernetics).

Small interfering RNA transfection

Before transfection, ECs were seeded into 6-well plates at a density of 2.5×10^5 cells/well and incubated overnight. For small interfering RNA (siRNA)-mediated gene knockdown, 50 nmol/L of mTOR siRNA SMARTpool, platelet endothelial cell adhesion molecule-1 (PECAM-1, PECAM, CD31) siRNA SMARTpool, vascular endothelial growth factor receptor 2 (VEGFR2) siRNA SMARTpool or control siRNA (Dharmacon, Chicago, IL, USA) were transfected into cells with DharmaFECT Transfection Reagent IV (Dharmacon) according to the manufacturer's protocol. After 72 hours of transfection, cells were harvested for further analysis.

Western blot analysis

Western blot analysis was performed as previously described (22). Briefly, ECs were lysed in Cell Lytic MT lysis buffer (Sigma-Aldrich) with Protease Inhibitor Cocktail (Invitrogen) for 15 minutes on a shaker. After centrifugation for 10 minutes at 12,000×g (4°C), the supernatants were saved and protein concentrations of the samples were determined using

the Pierce BCA Protein Assay Kit (Thermo Scientific, Waltham, MA, USA). Equal amounts of protein (30 μg) were loaded onto SDS-polyacrylamide gels and blotted onto PVDF membranes (BioRad, Hercules, CA, USA). Western blots analysis used antibodies against mTOR downstream S6, and p-S6 (rabbit monoclonal antibodies, 1:1,000, Cell Signaling, Beverly, MA, USA), PECAM-1 (rabbit polyclonal anti-PECAM-1, 1:1,000, Abcam, Cambridge, MA, USA) and intercellular adhesion molecule-2 (ICAM-2) (rabbit polyclonal anti-ICAM-2, 1:200, Santa Cruz, Dallas, Texas, USA). Antibody against β-actin (rabbit monoclonal anti-β-actin, 1:2,000, Cell Signaling) was used as a loading control. For detection, the membrane was incubated with anti-rabbit IgG secondary antibodies conjugated with horseradish peroxidase (1:2,000, Cell Signaling). Bands were visualized using SuperSignal West Pico Chemiluminescent substrate (ThermoScientific Pierce, Rockford, IL, USA).

Annexin V staining

Dual staining with FITC–annexin V and propidium iodide (PI) was performed to detect cells undergoing apoptosis using an annexin V–FITC kit (BD Biosciences) as we described previously (10). Single lung cells were first stained with endothelial marker CD31. After washing with PBS, labeled cells were resuspended in annexin V-binding buffer containing FITC-conjugated annexin V. PI was then added into cells and incubated on ice for 10 min. Nonspecific binding was blocked by pre-incubating cells with rat IgG (10 mg/mL) and anti-FcII/III. Cells were analyzed on a LSRII machine (Becton Dickinson, Franklin Lakes, New Jersey, USA) within 1 h. Viable cells were defined by $FITC^{-}$ and PI^{-} population. Early apoptotic cells were defined by $FITC^{+}$ and PI^{-} population.

In vitro co-culture of ECs and MDSCs

ECs were resuspended and adjusted to density at 5×10^{4} cells/mL. MDSCs after MACS sorting were used immediately and the cell density was adjusted to 5×10^{6} cells/mL. One hundred microliters of MDSCs and 100 μL of ECs were mixed, and seeded into a well of 96-well plates. Seventy-two hours later, unattached MDSCs were removed by washing with PBS, and the number of attached ECs was counted. Morphologically, MDSCs are much smaller than ECs.

BrdU incorporation

Immunofluorescent staining of incorporated bromodeoxyuridine (BrdU) was also performed on ECs after coculture with MDSCs for 3 days and washing off the MDSCs by PBS, followed by flow cytometric analysis. BrdU incorporation was performed using the BrdU Flow Kit (BD Biosciences) as we previously described (10). Briefly, BrdU was added to cells at a final concentration of 10 μmol/L. One hour later, cells were collected and fixed. After permeabilisation, cells were incubated with DNase I at 37°C for 1 h, followed by labeling with anti-BrdU antibody for 20 min at room temperature. Cells were then analyzed by flow cytometry.

In vivo matrigel plug assay with ECs or MDSCs

This assay was performed according to established methods with minor modifications (25). ECs or MDSCs were collected separately. After washed with PBS, 1×10^6 ECs or 2×10^6 MDSCs were centrifuged and resuspended in 40 μL PBS and mixed with 500 μL Matrigel Basement Membrane Matrix (BD Biosciences) containing 15 units of heparin (Sigma-Aldrich). The cell-matrigel-mixture was then injected subcutaneously into the abdomen of 3-month old *lal*$^{+/+}$ mice. For the B16 melanoma tumor model, 1×10^6 MDSCs and 1×10^5 B16 melanoma cells were mixed in 500 μL matrigel, and then injected subcutaneously into *lal*$^{+/+}$ mice. After 10 days, the mice were sacrificed and plugs were harvested from underneath the skin. The plugs were fixed, embedded, sectioned, stained with H&E, and then examined using microscopy. To visualize capillaries, samples were immunohistochemically stained with anti-CD31 antibody. For hemoglobin analysis, the matrigel plugs were removed after 10 days and homogenized in 130 μL de-ionized water. After centrifugation, the supernatant was harvested, and then used in the Drabkin assay (Sigma-Aldrich) to measure hemoglobin concentration. Stock solutions of hemoglobin are used to generate a standard curve. Results are expressed relative to total protein in the supernatant.

T cell proliferation assay and lymphokine measurement by ELISA

$CD4^+$ T cells were prepared and CFSE labeled as we previously described (26). Labeled $CD4^+$ T cells were co-cultured with ECs in 96-well plates pre-coated with anti-CD3 monoclonal antibody (mAb) (2 μg/mL) and anti-CD28 mAb (5 μg/mL) at 37°C, 5% CO_2 for 4 d. The ratio of ECs/$CD4^+$ T cells was 1:10. Proliferation of $CD4^+$ T cells was evaluated as CFSE dilution by FACS. The expression level of IL-4, IL-10, IFN-γ, and IL-17 in the supernatants of the culture medium was measured using ELISA kits (BD Biosciences).

Real-time RT-PCR

Total RNAs from ECs or $Ly6G^+$ cells were purified using the Qiagen total RNA purification kit (Qiagen, Valencia, CA, USA). Quantitative (q)RT-PCR was performed as described previously (20). Analysis was performed by the $2^{-\Delta\Delta CT}$ method. Primers of mMCP-1, mCCR2, mIL-6, mTNF-α, VEGF and GAPDH for real-time PCR were described previously (20).

Flow Cytometry Analysis

After 7 days of culture, ECs were harvested and washed with PBS. To detect VEGFR-2 expression level, cells were incubated with APC-conjugated anti-mouse VEGFR-2 antibody (eBioscience, San Diego, CA, USA). For flow cytometry analysis, ≥10,000 cells were acquired and scored using a LSRII machine (Becton Dickinson). Data were processed using the CellQuest software program (Becton Dickinson).

ROS Measurement

The reactive oxygen species (ROS) level in ECs was measured by flow cytometry as we previously described (13). Briefly, ECs were harvested, washed, and stained with 2 μmol/L 2′, 7′-dichlorofluorescein diacetate (Invitrogen) at 37°C for 30 min. After PBS wash, the

ROS level was analyzed using a LSRII machine (Becton Dickinson). In a ROS inhibition assay, the antioxidant *N*-Acetyl-L-cysteine (NAC) (Sigma-Aldrich) was added to ECs twice per day for 3 days, followed by further analysis.

Statistics

Data were expressed as mean ± SD. Differences between two treatment groups were compared by Student's *t*-test. When more than two groups were compared, one-way ANOVA with post-hoc Newman-Keul's multiple comparison test was used. Results were considered statistically significant when $P < 0.05$. All analyses were performed with GraphPad Prism 5.0 (GraphPad, San Diego, CA, USA).

Results

LAL deficiency in ECs led to increased transendothelial migration of MDSCs

Transendothelial migration of leukocytes is a critical step in the inflammatory response, during which ECs participate in regulating leukocyte transmigration from the vasculature to the site of inflammation (27). Because we have previously reported that LAL deficiency results in severe infiltration of MDSCs in multiple organs (1, 10, 12, 28, 29), the role of ECs in MDSC infiltration was investigated. Transwell assay was performed to determine MDSC transmigration across the endothelial monolayer formed by ECs isolated from lungs of $lal^{+/+}$ or $lal^{-/-}$ mice. ECs were seeded into Transwell upper chambers and grown to confluence. Freshly isolated bone marrow-derived $Ly6G^+$ cells (MDSCs) from $lal^{+/+}$ or $lal^{-/-}$ mice were labeled with CMFDA and then loaded on the EC monolayers. In $lal^{-/-}$ mice, since almost all $Ly6G^+$ cells are positive for CD11b, which showed T cell suppression, Ly6G antibody was used for purification of $Ly6G^+CD11b^+$ cells (30). Six hours later, the number of $Ly6G^+$ cells that had migrated to the lower chamber was counted. As shown in Figure 1A, when $lal^{+/+}$ $Ly6G^+$ cells were added to the EC monolayer, $lal^{-/-}$ ECs showed increased permeability, with more $Ly6G^+$ cells in the lower chamber, than that of $lal^{+/+}$ ECs. In addition, we repeated the experiments using $lal^{-/-}$ $Ly6G^+$ cells to migrate across $lal^{+/+}$ or $lal^{-/-}$ EC monolayers, and there were more $lal^{-/-}$ $Ly6G^+$ cells migrating to the lower chamber through $lal^{-/-}$ ECs than $lal^{+/+}$ ECs. These data suggest that 1) the increased permeability of $lal^{-/-}$ ECs is a potential mechanism of increased $Ly6G^+$ cell infiltration in the $lal^{-/-}$mice and 2) $lal^{-/-}$ $Ly6G^+$ cells possess a stronger ability to transmigrate the pulmonary EC monolayer. As a matter of fact, $lal^{-/-}$ $Ly6G^+$ cell and $lal^{-/-}$ EC combination showed three times more permeability than that of $lal^{+/+}$ $Ly6G^+$ cell and $lal^{+/+}$ EC combination. In addition to $Ly6G^+$ cells, $lal^{-/-}$ $CD4^+$ T cells also showed increased ability of transendothelial migration, with similar results as $Ly6G^+$ cells (Figure 1B).

A number of adhesion molecules have been implicated in the process of leukocyte transendothelial migration (27). It is plausible that increased expression of adhesion molecules in $lal^{-/-}$ ECs facilitates $Ly6G^+$ cell transmigration across the endothelial monolayer. Among several tested proteins, Western blot analysis showed that expression of PECAM-1 and ICAM-2 was both elevated in $lal^{-/-}$ ECs (Figure 1C). To assess functional roles of PECAM-1 in ECs for $Ly6G^+$ cell transendothelial migration, siRNA transfection was performed to knockdown PECAM-1 expression in ECs. Results of Transwell assay

showed that there were less migrated Ly6G$^+$ cells in the groups of *lal*$^{+/+}$ and *lal*$^{-/-}$ ECs with PECAM-1 siRNA transfection than their counterparts with control siRNA transfection (Figure 1D). Furthermore, ECs were treated with anti-PECAM-1 neutralizing antibodies. As Figure 1E demonstrated, the transmigration of Ly6G$^+$ cells across the EC monolayer was reduced in the groups of ECs with anti-PECAM-1 antibody treatment compared to those treated with control IgG. Taken together, increased expression of PECAM-1 in *lal*$^{-/-}$ ECs contributed to enhanced Ly6G$^+$ cell transmigration.

Moreover, chemokines secreted by ECs are crucial in recruiting monocytes into the vessel wall, among which MCP-1 plays a major role (31, 32). In *lal*$^{-/-}$ ECs, the mRNA level of MCP-1 was up-regulated by a Real-time PCR analysis (Figure 1F). Accordingly, expression of MCP-1 receptor - CCR2 was increased in *lal*$^{-/-}$ Ly6G$^+$ cells (Figure 1G). To examine whether MCP-1 secreted by *lal*$^{-/-}$ ECs facilitated Ly6G$^+$ cell migration, transwell study was performed with ECs pre-treated with anti-MCP-1 neutralizing antibodies. As shown in Figure 1H, fewer Ly6G$^+$ cells transmigrated through ECs treated with anti-MCP-1 antibody than those treated with control IgG. In addition, the mRNA levels of IL-6 and TNFα were increased in *lal*$^{-/-}$ ECs (Figure 1F), both of which have been reported to be involved in EC permeability (33, 34). After ECs were pre-treated with anti-IL-6 or anti-TNFα antibodies to neutralize cytokines, Ly6G$^+$ cell transmigration was not significantly inhibited. However, combination of all three neutralizing antibodies (anti-MCP-1, anti-IL-6 and anti-TNFα antibodies) showed a stronger blocking on Ly6G$^+$ cell transmigration (Figure 1H). Therefore, chemokines and cytokines, especially MCP-1, secreted by *lal*$^{-/-}$ ECs are responsible for mediating Ly6G$^+$ cell transendothelial migration.

LAL deficiency influenced EC angiogenic functions

Angiogenesis is a feature of chronic inflammation, a process ECs actively participate in (3). Three studies were designed to assess angiogenic functions. Firstly, an important aspect of angiogenesis involves the formation of capillary-like tubes by ECs (35). To determine whether LAL deficiency influences tube formation, *in vitro* matrigel tube formation assay was performed. As shown in Figure 2A, 6 h after seeding on matrigel, *lal*$^{-/-}$ ECs formed significantly less completed and poorly connected tube networks than those of *lal*$^{+/+}$ ECs. Statistical results showed that there was more than 50% decrease in the total tube lengths in *lal*$^{-/-}$ ECs compared with those of *lal*$^{+/+}$ ECs, demonstrating that LAL deficiency impaired EC tube formation *in vitro*. Interestingly, tube networks formed by *lal*$^{-/-}$ ECs showed a delayed disappearance compared with those formed by *lal*$^{+/+}$ ECs at 12h and 24h.

Secondly, we investigated the effect of LAL deficiency on EC-mediated *in vivo* angiogenesis by *in vivo* matrigel plug assay. Fourteen days after subcutaneous injection of EC-matrigel-mixture, the mice were sacrificed and plugs were harvested, sectioned, and stained with H&E. The presence of capillaries in the matrigel was further detected by immunohistochemical (IHC) staining with anti-CD31 antibody. Results showed that administration of *lal*$^{+/+}$ ECs induced formation of vessel-like structures and the presence of erythrocytes were evidenced in the lumen (Figure 2B, see arrows), while administration of *lal*$^{-/-}$ ECs led to formation of disorganized cell clusters, demonstrating that LAL deficiency in ECs impaired their *in vivo* angiogenic function. As a control, plugs without ECs showed

no vessel formation or $CD31^+$ cells (data not shown), confirming that the above observations were from extrinsic ECs. In addition, the hemoglobin content (a surrogate marker of perfusion) was significantly lowered in the plugs mixed with $lal^{-/-}$ ECs (Figure 2C).

Thirdly, endothelial cell migration is an essential component of angiogenesis (36). To test whether LAL deficiency in ECs affects their migration ability, we performed the *in vitro* wound healing assay. ECs were treated with mitomycin C to eliminate the potential effects of EC proliferation. As shown in Figure 2D, 15 h after creating the scratch, $lal^{-/-}$ ECs demonstrated increased migration compared with that of $lal^{+/+}$ ECs, evidenced by a significant reduction in the wound area lacking cells. This indicates that LAL deficiency facilitates EC migration.

LAL deficiency facilitated EC proliferation

Cell proliferation is essential for ECs to adequately perform their functions. Therefore, the effect of LAL deficiency on EC proliferation was determined. $CD31^+$ ECs from the lungs of $lal^{+/+}$ or $lal^{-/-}$ mice were isolated and counted. There were significantly more $CD31^+$ cells in the lungs of $lal^{-/-}$ mice than those in the lungs of $lal^{+/+}$ mice (Figure 3A). When cultured *in vitro*, $lal^{-/-}$ ECs demonstrated increased proliferation compared with that of $lal^{+/+}$ ECs (Figure 3B). The BrdU incorporation study further supported increased proliferation of $lal^{-/-}$ ECs (Figure 3C). Since apoptosis may contribute to the numbers of ECs, we further examined the apoptotic activity in isolated lung ECs by Annexin V staining. The percentage of Annexin V positive cells in lung $CD31^+$ cells was compared between $lal^{+/+}$ and $lal^{-/-}$ mice. As shown in Figure 3D, apoptosis in $lal^{-/-}$ lung $CD31^+$ cells was decreased compared with those of $lal^{+/+}$ mice. The abnormality of $lal^{-/-}$ EC proliferation is a complicated process, which can be influenced by environmental factors. In addition to the above intrinsic defects in ECs, we also investigated the effect of blood plasma on EC proliferation. Plasma was prepared from both $lal^{+/+}$ and $lal^{-/-}$ blood, and added into culture medium (20% plasma) of ECs. Seventy-two hours later, $lal^{-/-}$ plasma exerted a greater stimulatory effect on both $lal^{+/+}$ and $lal^{-/-}$ EC proliferation, compared with that of $lal^{+/+}$ plasma (Figure 3E). Since $lal^{-/-}$ ECs showed more sensitivity to plasma treatment, the potential mechanism contributing to EC growth was investigated. VEGF has been found to have various functions on ECs, the most prominent of which is the stimulation of proliferation and angiogenesis (37, 38). The VEGF level was indeed increased in $lal^{-/-}$ plasma (data not shown). Therefore, the level of its receptor VEGFR2 was examined in $lal^{+/+}$ vs. $lal^{-/-}$ ECs. Flow cytometry analysis showed that the expression level of VEGFR2 was increased in $lal^{-/-}$ ECs (Figure 3F). After VEGFR2 knockdown in ECs, the stimulatory effect of $lal^{-/-}$ plasma on EC proliferation was impaired (Figure 3G). These results indicate that both intrinsic defects and environmental factors contribute to abnormal proliferation of $lal^{-/-}$ ECs.

LAL deficiency in ECs suppressed T cell proliferation

Increased T cell permeability across the ECs monolayer (Figure 1B) triggered us to further investigate ECs' effects on T cell proliferation and functions. ECs have been found to function as antigen presentation cells, leading to activation of T cells (39, 40). We have previously reported that LAL deficiency impaired T cell proliferation and function in $lal^{-/-}$

mice (26). Although the intrinsic defect and *lal*$^{-/-}$ MDSC suppression contribute to T cell paucity (26), whether *lal*$^{-/-}$ ECs participate in T cell suppression has not been investigated. CFSE-labeled *lal*$^{+/+}$ CD4^{+} T cells were cultured *in vitro* and stimulated with anti-CD3 mAb plus anti-CD28 mAb in the presence or absence of *lal*$^{+/+}$ or *lal*$^{-/-}$ ECs for 4 d. Proliferation of CD4^{+} T cells was evaluated by CFSC dilution (cell division). As demonstrated in Figure 4A, *lal*$^{-/-}$ ECs showed inhibition on proliferation of *lal*$^{+/+}$ CD4^{+} T cells after anti-CD3 mAb plus anti-CD28 mAb stimulation, whereas *lal*$^{+/+}$ ECs had no effects on CD4^{+} T cell proliferation. In the PBS control group, no proliferation was observed. Furthermore, the secretion of CD4^{+} T lymphokines, e.g. IFN-γ (Th1), IL-4 and IL-10 (Th2) was also inhibited by *lal*$^{-/-}$ ECs, while the secretion of Th17 lymphokine IL-17 remained unchanged (Figure 4B). Therefore, *lal*$^{-/-}$ ECs suppressed both T cell proliferation and lymphokine secretion.

Interaction with MDSCs leads to EC dysfunctions

Our previous publications have demonstrated that the MDSC population in *lal*$^{-/-}$ mice was significantly increased in multiple organs (10-12). The synergism between Ly6G^{+} cells and ECs in the *lal*$^{-/-}$ mice has been implicated in Figure 1A, in which not only *lal*$^{-/-}$ ECs had enhanced permeability for Ly6G^{+} cells, but also *lal*$^{-/-}$ Ly6G^{+} cells had greater transmigration capability than that of *lal*$^{+/+}$ Ly6G^{+} cells. It is intriguing to determine if *lal*$^{-/-}$ Ly6G^{+} cells influence EC proliferation and functions. To test whether Ly6G^{+} cells contribute to angiogenesis, the EC tube formation assay was performed in the presence of Ly6G^{+} cells. In this study, both *lal*$^{+/+}$ and *lal*$^{-/-}$Ly6G^{+} cells facilitated *lal*$^{-/-}$ EC tube formation (Figure 5A). Despite impaired tube formation in the absence of Ly6G^{+} cells, *lal*$^{-/-}$ ECs co-cultured with *lal*$^{-/-}$ Ly6G^{+} cells formed more complete tube networks than those with *lal*$^{+/+}$ Ly6G^{+} cells, suggesting that *lal*$^{-/-}$ Ly6G^{+} cells exert proangiogenic effects on ECs. However, when ECs were co-cultured with macrophages (F4/80^{+} and CD11b^{+}) that were isolated from *lal*$^{+/+}$ or *lal*$^{-/-}$ mice, *lal*$^{+/+}$ macrophages stimulated tube formation on ECs, while *lal*$^{-/-}$ macrophages did not (Figure 5B). This difference indicates differential abilities between *lal*$^{+/+}$ and *lal*$^{-/-}$ macrophages to stimulate EC tube formation. In a similar study, both *lal*$^{+/+}$ and *lal*$^{-/-}$ CD4^{+} T cells showed no effect on EC tube formation (Figure 5B).

In the *in vivo* matrigel plug assay, matrigel mixed with either *lal*$^{+/+}$ or *lal*$^{-/-}$ Ly6G^{+} cells were injected into *lal*$^{+/+}$ mice subcutaneously. Fourteen days after implantation, matrigel plugs containing *lal*$^{-/-}$ Ly6G^{+} cells showed more CD31^{+} cells than those containing *lal*$^{+/+}$ Ly6G^{+} cells. H&E staining results revealed newly formed microvessels in the plugs containing *lal*$^{-/-}$ Ly6G^{+} cells (Figure 5C, see arrows). The effect of Ly6G^{+} cells on angiogenesis *in vivo* was further examined in a B16 melanoma tumor model, a system that was recently established by us (14). *lal*$^{+/+}$ or *lal*$^{-/-}$ Ly6G^{+} cells were isolated and mixed with B16 melanoma cells in matrigel. The mixture was subcutaneously injected into wild type recipient mice for tumor growth study. IHC staining showed that more CD31^{+} cells appeared in matrigel plugs containing *lal*$^{-/-}$ Ly6G^{+} cells than those containing *lal*$^{+/+}$ Ly6G^{+} cells (Figure 5D). The underlying mechanism of this proangiogenic activity was further investigated. The mRNA level of VEGF, a crucial factor in regulating EC angiogenesis, was up-regulated in *lal*$^{-/-}$ Ly6G^{+} cells (Figure 5E). On the other hand, inhibition of VEGF receptor 2 (VEGFR2) expression by siRNA knockdown in ECs decreased the tube-forming

activity by *lal*$^{-/-}$ Ly6G^{+} cells (Figure 5F), suggesting that VEGF secreted by *lal*$^{-/-}$ Ly6G^{+} cells is responsible for the pro-angiogenic activity.

The effect of Ly6G^{+} cells on EC proliferation was also determined. ECs were co-cultured with *lal*$^{+/+}$ or *lal*$^{-/-}$ Ly6G^{+} cells for 72 h, and the numbers of ECs were counted. As shown in Figure 5G, ECs co-cultured with *lal*$^{-/-}$ Ly6G^{+} cells showed more proliferative cells than those with *lal*$^{+/+}$ Ly6G^{+} cells. *lal*$^{-/-}$ ECs co-cultured with *lal*$^{-/-}$ Ly6G^{+} cells showed the highest proliferation, which was consistent with Figure 3A, in which proliferation of CD31^{+} cells was increased in *lal*$^{-/-}$ mice. This observation was further supported by BrdU incorporation assay, showing significant increase of BrdU incorporation when ECs were co-cultured with *lal*$^{-/-}$ Ly6G^{+} cells (Figure 5H).

Over-activation of the mTOR pathway is responsible for EC dysfunctions

In *lal*$^{-/-}$ mice, over-activation of the mTOR pathway has been identified in bone marrow-derived MDSCs (13, 14, 17). Interestingly, Western blot analysis also detected increased level of phosphorylated-S6, a downstream target protein of mTOR (41), in *lal*$^{-/-}$ ECs (Figure 6A). Knocking down mTOR expression in *lal*$^{-/-}$ ECs by siRNA transfection showed significant decrease of phosphorylated-S6 compared with *lal*$^{-/-}$ ECs transfected with control siRNA (Figure 6B). These results implied pathogenic roles of mTOR over-activation in *lal*$^{-/-}$ ECs. To see if the mTOR pathway plays roles in *lal*$^{-/-}$ EC dysfunctions, the effect of mTOR inhibition in *lal*$^{-/-}$ ECs on Ly6G^{+} cell transendothelial migration was analyzed by Transwell assay. After ECs were transfected with mTOR or control siRNA for 48 h, Ly6G^{+} cells were added to the *lal*$^{+/+}$ or *lal*$^{-/-}$EC monolayer. Six hours later, the number of Ly6G^{+} cells in the lower chamber was significantly less across both *lal*$^{+/+}$ and *lal*$^{-/-}$ ECs transfected with mTOR siRNA than those across ECs with control siRNA transfection (Figure 6C), suggesting that mTOR inhibition in ECs reduces Ly6G^{+} cell transendothelial migration. Furthermore, the *in vitro* wound healing assay showed delayed migration towards the scratch in *lal*$^{-/-}$ ECs with mTOR siRNA transfection at 12 h and 18 h after creating the scratch, with a significant increase of distance in the wounding area (Figure 6D), indicating mTOR inhibition impairs the increased migration of *lal*$^{-/-}$ ECs. Finally, mTOR inhibition in *lal*$^{-/-}$ ECs reversed their suppressive activity on T cells. As demonstrated in Figure 6E, *lal*$^{-/-}$ ECs with control siRNA transfection showed inhibition on T cell proliferation, whereas *lal*$^{-/-}$ ECs with mTOR siRNA transfection displayed reduced inhibition on T cell proliferation. *lal*$^{-/-}$ ECs with mTOR siRNA transfection also reversed decreased secretion of IL-4, IL-10 and IFN-γ by T cells (Figure 6F).

Over-production of ROS mediates the over-activation of mTOR pathway in EC dysfunction

ROS over-production has been observed, and rapamycin treatment decreased the ROS level in *lal*$^{-/-}$ Ly6G^{+} MDSCs (13, 17). Similarly, the ROS level was also increased in *lal*$^{-/-}$ ECs, and rapamycin treatment suppressed ROS production in *lal*$^{-/-}$ ECs (Figure 7A). To see if the ROS over-production mediates the mTOR signaling in EC dysfunctions, ECs were treated with antioxidant NAC to neutralize ROS. In the transendothelial migration study, NAC pre-treatment of ECs significantly reduced both *lal*$^{+/+}$ and *lal*$^{-/-}$ Ly6G^{+} cell migration across the ECs monolayer (Figure 7B). The same EC treatment also improved tube formation of *lal*$^{-/-}$ ECs (Figure 7C), and delayed *lal*$^{-/-}$ EC migration towards the scratch

with a significant increase of distance in the wounding area in the *in vitro* wound healing assay (Figure 7D). NAC treatment reduced $lal^{-/-}$ EC proliferation (Figure 7E). Finally, NAC pre-treatment of $lal^{-/-}$ ECs reversed their suppressive activity on T cell proliferation (Figure 7F). Taken together, these results support a concept that ROS over-production serves as a mechanism mediating mTOR over-activation in $lal^{-/-}$ EC dysfunctions.

Discussion

LAL is a key enzyme in the metabolic pathway of neutral lipids, and the relationship between LAL and inflammation has been well documented (1, 10-14, 28). Genetic ablation of the *lal* gene in mice has resulted in a systemic increase of MDSCs, causing severe inflammation and pathogenesis in multiple organs (10). ECs, the major components of blood vessels, are actively involved in inflammation and many other pathogenic conditions. However, the effects of LAL deficiency on EC functions remain to be explored. The major new findings of the present study were that LAL deficiency in ECs 1) enhanced the transendothelial migration of MDSCs, with a concomitant increase of PECAM-1 and ICAM-2 protein levels, 2) impaired *in vitro* tube-forming capability and *in vivo* angiogenesis, but increased migration, 3) facilitated cell proliferation, paralleled with reduced apoptosis, and 4) suppressed T cell proliferation and function. The potential mechanisms underlying EC dysfunction were identified, including the interaction with MDSCs, intrinsic over-activation of the mTOR pathway, and cellular overproduction of ROS. $lal^{-/-}$ MDSCs were found to increase transmigration across EC monolayers, promote *in vivo* angiogenesis, and EC tube formation and proliferation. The mTOR pathway was over-activated in $lal^{-/-}$ ECs, and inhibition of mTOR in $lal^{-/-}$ ECs partially reversed their dysfunctions, including reducing transmigration of MDSCs, EC migration, and suppression of T cell proliferation and function, which was mediated by decreasing ROS production.

Transendothelial migration of leukocytes, or diapedesis, is a critical step in the inflammatory response. The preceding steps of leukocyte rolling, activation, adhesion, and locomotion are all reversible. However, once the leukocytes commit to diapedesis, they do not return to the circulation, at least not as the same cell type (27, 42). Recent studies have shown that transendothelial migration was promoted by multiple endothelium-derived inflammatory chemokines (43, 44). Because we previously observed increased MDSC accumulation in the lungs of $lal^{-/-}$ mice (1, 10, 12), we hypothesized that LAL deficiency in ECs would enhance transendothelial migration of MDSCs. In consistence with our hypothesis, MDSCs migrated more efficiently across $lal^{-/-}$ ECs than $lal^{+/+}$ ECs. In addition, $lal^{-/-}$ MDSCs showed a greater transmigration capability than that of $lal^{+/+}$ MDSCs (Figure 1A). There was a more than 3-fold increase in the transmigration of $lal^{-/-}$ MDSCs across $lal^{-/-}$ ECs than that of $lal^{+/+}$ MDSCs across $lal^{+/+}$ ECs, which mimicked the pathological condition of $lal^{-/-}$ mice. Our finding demonstrated that in $lal^{-/-}$ mice, not only myeloid cells but also pulmonary ECs contribute to the increased transendothelial migration, which may explain the increased accumulation of myeloid cells in the bronchoalveolar lavage fluid of $lal^{-/-}$ mice (10).

Several mechanisms are involved in the process of transendothelial migration, among which is the hemophilic interaction of leukocyte PECAM with endothelial PECAM (27). PECAM-1 is an immunoglobulin superfamily member concentrated at the borders of ECs,

as well as diffusely on platelets and leukocytes. Study has shown that when PECAM-PECAM interactions are blocked, leukocytes are arrested tightly adherent to the apical surface of the cell (27, 45). In the present study, we found that PECAM-1 protein level was increased in *lal*$^{-/-}$ ECs (Figure 1C) and inhibition of PECAM-1 in ECs by siRNA transfection or neutralizing antibodies led to reduced transendothelial migration of *lal*$^{-/-}$ MDSCs (Figure 1D-E), which were consistent with previous findings, suggesting that the elevated expression of PECAM-1 in *lal*$^{-/-}$ ECs is critical for the enhanced transendothelial migration. We also found that ICAM-2 protein level was increased in *lal*$^{-/-}$ ECs, whose deletion has been reported to inhibit transmigration of neutrophils (46, 47). In addition to adhesion molecules in facilitating transendothelial migration of leukocytes, chemokines play an important role in recruiting monocytes, neutrophils, and lymphocytes to the vascular endothelium. MCP-1, acting through its receptor CCR2, has been demonstrated to recruit monocytes into foci of inflammation (48). The increased level of MCP-1 in *lal*$^{-/-}$ ECs and CCR2 in *lal*$^{-/-}$ Ly6G^{+} cells was observed (Figure 1F-G). Pre-treatment of ECs with anti-MCP-1 neutralizing antibodies reduced Ly6G^{+} cell transmigration by about 50% (Figure 1H). Furthermore, increased production of cytokines IL-6 and TNFα in *lal*$^{-/-}$ ECs has been observed, and combination of all three neutralizing antibodies further blocked Ly6G^{+} cell transmigration (Figure 1F and 1H), demonstrating up-regulated production of chemokines and cytokines in *lal*$^{-/-}$ ECs is responsible for mediating Ly6G^{+} cell transendothelial migration.

Angiogenesis, the growth of new capillaries from preexisting blood vessels, is a feature of chronic inflammation. ECs are the principle cell population participating in this complex process, which involves EC activation, disruption of vascular basement membranes, migration and proliferation of ECs, and the subsequent formation and maturation of blood vessels (49). Failure of ECs to adequately perform their angiogenesis-related functions would lead to an imbalance of the angiogenic process, resulting in the pathogenesis of numerous disorders (50). An important aspect of angiogenesis involves the organization of ECs into three-dimensional tube-like structures. Our results showed that LAL deficiency enhanced EC migration (Figure 2D), impaired EC tube formation (Figure 2A), and decreased *in vivo* angiogenesis by matrigel plug assay (Figure 2B-C).

During the process of angiogenesis, EC proliferation is required to provide the necessary number of cells for new blood vessel formation (51). However, increased EC proliferation is often related to pathological conditions. In *lal*$^{-/-}$ mice, it seems that both intrinsic defects and environmental factors contribute to EC proliferation. We observed that there were more pulmonary CD31^{+} cells, with significantly decreased apoptosis (Figure 3A and 3D). After *in vitro* culture, *lal*$^{-/-}$ ECs showed enhanced proliferation (Figure 3B-C). Furthermore, EC proliferation was greatly increased in the presence of plasma harvested from *lal*$^{-/-}$ mice. *lal*$^{-/-}$ECs co-cultured with plasma from *lal*$^{-/-}$ mice, a mimic of the *in vivo* situation of *lal*$^{-/-}$ mice, showed the greatest proliferation compared with other groups (Figure 3E), which was in agreement with the *in vivo* observation that more CD31^{+} cells existed in the lungs of *lal*$^{-/-}$ mice (Figure 3A). In addition, the up-regulated expression of VEGFR2 in *lal*$^{-/-}$ ECs was responsible for their higher response to the environmental factors since VEGFR2 knockdown in *lal*$^{-/-}$ ECs impaired the stimulatory effect of *lal*$^{-/-}$ plasma on their

proliferation (Figure 3 F-G). Collectively, the above observations suggest that LAL deficiency facilitates EC proliferation and inhibits EC apoptosis, despite the fact that *lal*$^{-/-}$ ECs had a poor capability of tube formation (Figure 2A) and *in vivo* capillary formation (Figure 2B).

ECs, which form the interface between the blood and the underlying tissue, are uniquely positioned for frequent contact with circulating T cells (23). In *lal*$^{-/-}$ mice, impairment in T cell proliferation and function has previously been reported (28). A recent study has found that direct cell-cell contact between ECs and T cells is required for EC-induced T cell proliferation (40). In our study, *lal*$^{-/-}$ ECs showed inhibition on T cell proliferation and lymphokine secretion (Figure 4), which is an additional cellular mechanism of the impaired T cell proliferation in *lal*$^{-/-}$ mice.

In *lal*$^{-/-}$ mice, one major manifestation is the massive expansion and infiltration of MDSCs into multiple organs (1, 2, 10, 12, 52). Therefore, we speculate that MDSCs from *lal*$^{-/-}$ mice interact with ECs and influence ECs' functions. Previously, MDSCs isolated from mouse tumors have been reported to induce *in vitro* angiogenesis by tube formation assay via producing angiogenic factors, including VEGF and bFGF (9). In the present study, we found that the tube-forming capability of *lal*$^{-/-}$ ECs was increased after co-culturing with *lal*$^{-/-}$ MDSCs (Figure 5A), and the pro-angiogenic effects of *lal*$^{-/-}$ MDSCs was mediated by increased production of VEGF (Figure 5E-F), suggesting that *lal*$^{-/-}$ MDSCs had the similar pro-angiogenic effects as tumor-derived MDSCs. The *in vivo* matrigel plug assay further confirmed the pro-angiogenic activity of *lal*$^{-/-}$ MDSCs (Figure 5C-D). Therefore, in *lal*$^{-/-}$ mice, compared with ECs' intrinsic angiogenic defect, the pro-angiogenic activity of *lal*$^{-/-}$ MDSCs contribute to the angiogenesis required for the process of inflammation. *lal*$^{-/-}$ MDSCs also facilitated EC proliferation (Figure 5C-D), which explains why more CD31^{+} cells existed in the lungs of *lal*$^{-/-}$ mice (Figure 3A). Taken together, MDSC expansion contributes to EC dysfunctions in *lal*$^{-/-}$ mice.

The mTOR pathway is a key regulator of cell growth and proliferation. Increasing evidence suggests that its dysregulation is associated with human diseases, including metabolic disease, neurodegeneration, aging, cancer, diabetes, and cardiovascular disease (53, 54). mTOR, defined as a regulatory kinase in ECs, plays an important role in EC survival, migration, and proliferation, and PI3K/AKT/mTOR signaling pathway may regulate PECAM-1 expression in mEC/EB derived ECs (16, 55). In the present study, we found that the phosphorylation level of mTOR downstream target S6 was significantly increased in *lal*$^{-/-}$ ECs, which can be reversed after mTOR knocking down by siRNA transfection. Knocking down mTOR in *lal*$^{-/-}$ ECs partially reversed EC dysfunctions, including decreasing the enhanced transmigration of MDSCs across *lal*$^{-/-}$ ECs, impairing the increased *lal*$^{-/-}$ ECs migrating capability and proliferation, and relieving the *lal*$^{-/-}$ ECs suppression on T cell proliferation and function (Figure 6C-F). We have recently reported that over-activation of the mTOR signaling leads to ROS over-production in *lal*$^{-/-}$ MDSCs (13). In the present study, ROS over-production was also observed in *lal*$^{-/-}$ ECs, which was reduced by mTOR inhibitor rapamycin. Neutralization of ROS by antioxidant NAC in *lal*$^{-/-}$ ECs reversed their dysfunctions (Figure 7), similar to those observed in mTOR studies. Therefore, ROS over-production serves as a major mechanism to mediate the mTOR

pathway in EC dysfunctions. The above findings provide a mechanistic basis for targeting MDSCs or mTOR or ROS to rejuvenate EC functions in LAL deficiency-related diseases. Clinically, LAL deficiency results in inherited recessive in-born error metabolic diseases: Wolman disease as the infantile on-set and cholesteryl ester storage disease (CESD) as the late on-set. Our *lal*$^{-/-}$ mice represent Wolman disease biochemically and CESD physiologically. Both enzyme therapy using recombinant human LAL (hLAL) protein and gene therapy using adenovirus-mediated hLAL expression have been successfully tested in *lal*$^{-/-}$ mouse model (56-58). It is conceivable that these strategies can be used to treat EC dysfunctions. In summary, our studies strongly support a concept that neutral lipid metabolism controlled by LAL plays a critical role in maintaining ECs' normal functions by regulation of MDSCs and the mTOR pathway.

Acknowledgments

We thank Miss Katlin L. Walls for animal maintenance and genotyping.

This work was supported by National Institutes of Health Grants CA138759, CA152099 (to C. Y.) and HL087001 (to H. D.).

Abbreviations used in this article

CMFDA	5-Chloromethylfluorescein Diacetate
ECs	endothelial cells
ICAM-2	intercellular adhesion molecule-2
LAL	lysosomal acid lipase
***lal*$^{+/+}$**	wild-type
***lal*$^{-/-}$**	LAL-deficient
MDSCs	myeloid-derived suppressor cells
mTOR	mammalian target of rapamycin
MCP-1	Monocyte chemoattractant protein 1
NAC	*N*-Acetyl-L-cysteine
PECAM-1	platelet endothelial cell adhesion molecule-1
PI	propidium iodide
ROS	reactive oxygen species
siRNA	small interfering RNA
VEGF	vascular endothelial growth factor
VEGFR2	vascular endothelial growth factor receptor 2

Reference

1. Lian X, Yan C, Yang L, Xu Y, Du H. Lysosomal acid lipase deficiency causes respiratory inflammation and destruction in the lung. Am J Physiol Lung Cell Mol Physiol. 2004; 286:L801–807. [PubMed: 14644759]
2. Lian X, Yan C, Qin Y, Knox L, Li T, Du H. Neutral lipids and peroxisome proliferator-activated receptor-{gamma} control pulmonary gene expression and inflammation-triggered pathogenesis in lysosomal acid lipase knockout mice. Am J Pathol. 2005; 167:813–821. [PubMed: 16127159]
3. Pober JS, Sessa WC. Evolving functions of endothelial cells in inflammation. Nat Rev Immunol. 2007; 7:803–815. [PubMed: 17893694]
4. Sica A, Bronte V. Altered macrophage differentiation and immune dysfunction in tumor development. J Clin Invest. 2007; 117:1155–1166. [PubMed: 17476345]
5. Ostrand-Rosenberg S, Sinha P. Myeloid-derived suppressor cells: linking inflammation and cancer. J Immunol. 2009; 182:4499–4506. [PubMed: 19342621]
6. Gabrilovich DI, Nagaraj S. Myeloid-derived suppressor cells as regulators of the immune system. Nature reviews. Immunology. 2009; 9:162–174.
7. Pan PY, Wang GX, Yin B, Ozao J, Ku T, Divino CM, Chen SH. Reversion of immune tolerance in advanced malignancy: modulation of myeloid-derived suppressor cell development by blockade of stem-cell factor function. Blood. 2008; 111:219–228. [PubMed: 17885078]
8. Yang L, DeBusk LM, Fukuda K, Fingleton B, Green-Jarvis B, Shyr Y, Matrisian LM, Carbone DP, Lin PC. Expansion of myeloid immune suppressor Gr+CD11b+ cells in tumor-bearing host directly promotes tumor angiogenesis. Cancer Cell. 2004; 6:409–421. [PubMed: 15488763]
9. Kujawski M, Kortylewski M, Lee H, Herrmann A, Kay H, Yu H. Stat3 mediates myeloid cell-dependent tumor angiogenesis in mice. J Clin Invest. 2008; 118:3367–3377. [PubMed: 18776941]
10. Qu P, Shelley WC, Yoder MC, Wu L, Du H, Yan C. Critical roles of lysosomal acid lipase in myelopoiesis. Am J Pathol. 2010; 176:2394–2404. [PubMed: 20348241]
11. Wu L, Du H, Li Y, Qu P, Yan C. Signal transducer and activator of transcription 3 (Stat3C) promotes myeloid-derived suppressor cell expansion and immune suppression during lung tumorigenesis. Am J Pathol. 2011; 179:2131–2141. [PubMed: 21864492]
12. Yan C, Lian X, Li Y, Dai Y, White A, Qin Y, Li H, Hume DA, Du H. Macrophage-specific expression of human lysosomal acid lipase corrects inflammation and pathogenic phenotypes in lal −/− mice. Am J Pathol. 2006; 169:916–926. [PubMed: 16936266]
13. Ding X, Du H, Yoder MC, Yan C. Critical role of the mTOR pathway in development and function of myeloid-derived suppressor cells in lal−/− mice. Am J Pathol. 2014; 184:397–408. [PubMed: 24287405]
14. Zhao T, Du H, Ding X, Walls K, Yan C. Activation of mTOR pathway in myeloid-derived suppressor cells stimulates cancer cell proliferation and metastasis in *lal*−/− mice. Oncogene. 2014 In press.
15. Guertin DA, Sabatini DM. Defining the role of mTOR in cancer. Cancer Cell. 2007; 12:9–22. [PubMed: 17613433]
16. Dormond O, Madsen JC, Briscoe DM. The effects of mTOR-Akt interactions on anti-apoptotic signaling in vascular endothelial cells. J Biol Chem. 2007; 282:23679–23686. [PubMed: 17553806]
17. Yan C, Ding X, Dasgupta N, Wu L, Du H. Gene profile of myeloid-derived suppressive cells from the bone marrow of lysosomal acid lipase knock-out mice. PLoS One. 2012; 7:e30701. [PubMed: 22383970]
18. Dong QG, Bernasconi S, Lostaglio S, Wainstok De Calmanovici R, Martin-Padura I, Breviario F, Garlanda C, Ramponi S, Mantovani A, Vecchi A. A General Strategy for Isolation of Endothelial Cells From Murine Tissues: Characterization of Two Endothelial Cell Lines From the Murine Lung and Subcutaneous Sponge Implants. Arteriosclerosis, Thrombosis, and Vascular Biology. 1997; 17:1599–1604.
19. Fehrenbach ML, Cao G, Williams JT, Finklestein JM, DeLisser HM. Isolation of murine lung endothelial cells. American Journal of Physiology - Lung Cellular and Molecular Physiology. 2009; 296:L1096–L1103. [PubMed: 19304908]

20. Wu L, Yan C, Czader M, Foreman O, Blum JS, Kapur R, Du H. Inhibition of PPARgamma in myeloid-lineage cells induces systemic inflammation, immunosuppression, and tumorigenesis. Blood. 2012; 119:115–126. [PubMed: 22053106]
21. Zhang X, Goncalves R, Mosser DM. The isolation and characterization of murine macrophages. Curr Protoc Immunol. 2008 Chapter 14: Unit 14 11.
22. Zhao T, Li J, Chen AF. MicroRNA-34a induces endothelial progenitor cell senescence and impedes its angiogenesis via suppressing silent information regulator 1. Am J Physiol Endocrinol Metab. 2010; 299:E110–116. [PubMed: 20424141]
23. Hamada H, Kim MK, Iwakura A, Ii M, Thorne T, Qin G, Asai J, Tsutsumi Y, Sekiguchi H, Silver M, Wecker A, Bord E, Zhu Y, Kishore R, Losordo DW. Estrogen Receptors α and β Mediate Contribution of Bone Marrow–Derived Endothelial Progenitor Cells to Functional Recovery After Myocardial Infarction. Circulation. 2006; 114:2261–2270. [PubMed: 17088460]
24. Liang C-C, Park AY, Guan J-L. In vitro scratch assay: a convenient and inexpensive method for analysis of cell migration in vitro. Nat. Protocols. 2007; 2:329–333.
25. Bonauer A, Carmona G, Iwasaki M, Mione M, Koyanagi M, Fischer A, Burchfield J, Fox H, Doebele C, Ohtani K, Chavakis E, Potente M, Tjwa M, Urbich C, Zeiher AM, Dimmeler S. MicroRNA-92a Controls Angiogenesis and Functional Recovery of Ischemic Tissues in Mice. Science. 2009; 324:1710–1713. [PubMed: 19460962]
26. Qu P, Du H, Wilkes DS, Yan C. Critical roles of lysosomal acid lipase in T cell development and function. Am J Pathol. 2009; 174:944–956. [PubMed: 19179613]
27. Muller WA. Mechanisms of Transendothelial Migration of Leukocytes. Circulation Research. 2009; 105:223–230. [PubMed: 19644057]
28. Qu P, Du H, Wang X, Yan C. Matrix metalloproteinase 12 overexpression in lung epithelial cells plays a key role in emphysema to lung bronchioalveolar adenocarcinoma transition. Cancer Res. 2009; 69:7252–7261. [PubMed: 19706765]
29. Qu P, Yan C, Blum JS, Kapur R, Du H. Myeloid-specific expression of human lysosomal acid lipase corrects malformation and malfunction of myeloid-derived suppressor cells in lal−/− mice. J Immunol. 2011; 187:3854–3866. [PubMed: 21900179]
30. Qu P, Du H, Li Y, Yan C. Myeloid-specific expression of Api6/AIM/Sp alpha induces systemic inflammation and adenocarcinoma in the lung. J Immunol. 2009; 182:1648–1659. [PubMed: 19155514]
31. Shi C, Pamer EG. Monocyte recruitment during infection and inflammation. Nat Rev Immunol. 2011; 11:762–774. [PubMed: 21984070]
32. Pasceri V, Chang J, Willerson JT, Yeh ETH. Modulation of C-Reactive Protein–Mediated Monocyte Chemoattractant Protein-1 Induction in Human Endothelial Cells by Anti-Atherosclerosis Drugs. Circulation. 2001; 103:2531–2534. [PubMed: 11382718]
33. Lo C-W, Chen M-W, Hsiao M, Wang S, Chen C-A, Hsiao S-M, Chang J-S, Lai T-C, Rose-John S, Kuo M-L, Wei L-H. IL-6 Trans-Signaling in Formation and Progression of Malignant Ascites in Ovarian Cancer. Cancer Res. 2011; 71:424–434. [PubMed: 21123455]
34. Jöhrer K, Janke K, Krugmann J, Fiegl M, Greil R. Transendothelial Migration of Myeloma Cells Is Increased by Tumor Necrosis Factor (TNF)-α via TNF Receptor 2 and Autocrine Up-Regulation of MCP-1. Clinical Cancer Research. 2004; 10:1901–1910. [PubMed: 15041705]
35. Arnaoutova I, Kleinman HK. In vitro angiogenesis: endothelial cell tube formation on gelled basement membrane extract. Nat. Protocols. 2010; 5:628–635.
36. Lamalice L, Le Boeuf F, Huot J. Endothelial Cell Migration During Angiogenesis. Circulation Research. 2007; 100:782–794. [PubMed: 17395884]
37. Gerber H-P, McMurtrey A, Kowalski J, Yan M, Keyt BA, Dixit V, Ferrara N. Vascular Endothelial Growth Factor Regulates Endothelial Cell Survival through the Phosphatidylinositol 3′-Kinase/Akt Signal Transduction Pathway: REQUIREMENT FOR Flk-1/KDR ACTIVATION. Journal of Biological Chemistry. 1998; 273:30336–30343. [PubMed: 9804796]
38. Coultas L, Chawengsaksophak K, Rossant J. Endothelial cells and VEGF in vascular development. Nature. 2005; 438:937–945. [PubMed: 16355211]
39. Choi J, Enis DR, Koh KP, Shiao SL, Pober JS. T lymphocyteendothelial cell interactions. Annu. Rev. Immunol. 2004; 22:683–709. [PubMed: 15032593]

40. Wheway J, Obeid S, Couraud PO, Combes V, Grau GE. The brain microvascular endothelium supports T cell proliferation and has potential for alloantigen presentation. PLoS One. 2013; 8:e52586. [PubMed: 23320074]
41. Hay N, Sonenberg N. Upstream and downstream of mTOR. Genes Dev. 2004; 18:1926–1945. [PubMed: 15314020]
42. Muller, W. PECAM: Regulating the start of diapedesis. In: Ley, K., editor. Adhesion Molecules: Function and Inhibition. Birkhäuser Basel; 2007. p. 201-220.
43. Thelen M, Stein JV. How chemokines invite leukocytes to dance. Nat Immunol. 2008; 9:953–959. [PubMed: 18711432]
44. Shulman Z, Alon R. Real-time analysis of integrin-dependent transendothelial migration and integrin-independent interstitial motility of leukocytes. Methods Mol Biol. 2012; 757:31–45. [PubMed: 21909904]
45. Liao F, Huynh HK, Eiroa A, Greene T, Polizzi E, Muller WA. Migration of monocytes across endothelium and passage through extracellular matrix involve separate molecular domains of PECAM-1. J Exp Med. 1995; 182:1337–1343. [PubMed: 7595204]
46. Huang MT, Larbi KY, Scheiermann C, Woodfin A, Gerwin N, Haskard DO, Nourshargh S. ICAM-2 mediates neutrophil transmigration in vivo: evidence for stimulus specificity and a role in PECAM-1-independent transmigration. Blood. 2006; 107:4721–4727. [PubMed: 16469869]
47. Woodfin A, Voisin MB, Imhof BA, Dejana E, Engelhardt B, Nourshargh S. Endothelial cell activation leads to neutrophil transmigration as supported by the sequential roles of ICAM-2, JAM-A, and PECAM-1. Blood. 2009; 113:6246–6257. [PubMed: 19211506]
48. Deshmane SL, Kremlev S, Amini S, Sawaya BE. Monocyte chemoattractant protein-1 (MCP-1): an overview. J Interferon Cytokine Res. 2009; 29:313–326. [PubMed: 19441883]
49. Folkman J. Fundamental concepts of the angiogenic process. Curr Mol Med. 2003; 3:643–651. [PubMed: 14601638]
50. Carmeliet P. Angiogenesis in life, disease and medicine. Nature. 2005; 438:932–936. [PubMed: 16355210]
51. Auerbach R, Lewis R, Shinners B, Kubai L, Akhtar N. Angiogenesis Assays: A Critical Overview. Clinical Chemistry. 2003; 49:32–40. [PubMed: 12507958]
52. Du H, Heur M, Duanmu M, Grabowski GA, Hui DY, Witte DP, Mishra J. Lysosomal acid lipase-deficient mice: depletion of white and brown fat, severe hepatosplenomegaly, and shortened life span. J Lipid Res. 2001; 42:489–500. [PubMed: 11290820]
53. Li W, Petrimpol M, Molle KD, Hall MN, Battegay EJ, Humar R. Hypoxia-Induced Endothelial Proliferation Requires Both mTORC1 and mTORC2. Circulation Research. 2007; 100:79–87. [PubMed: 17110594]
54. Laplante M, Sabatini David M. mTOR Signaling in Growth Control and Disease. Cell. 2012; 149:274–293. [PubMed: 22500797]
55. Kim GD, Oh J, Jeong LS, Lee SK. Thio-Cl-IB-MECA, a novel A3 adenosine receptor agonist, suppresses angiogenesis by regulating PI3K/AKT/mTOR and ERK signaling in endothelial cells. Biochemical and Biophysical Research Communications. 2013; 437:79–86. [PubMed: 23791876]
56. Du H, Schiavi S, Levine M, Mishra J, Heur M, Grabowski GA. Enzyme therapy for lysosomal acid lipase deficiency in the mouse. Hum Mol Genet. 2001; 10:1639–1648. [PubMed: 11487567]
57. Du H, Heur M, Witte DP, Ameis D, Grabowski GA. Lysosomal acid lipase deficiency: correction of lipid storage by adenovirus-mediated gene transfer in mice. Hum Gene Ther. 2002; 13:1361–1372. [PubMed: 12162818]
58. Du H, Cameron TL, Garger SJ, Pogue GP, Hamm LA, White E, Hanley KM, Grabowski GA. Wolman disease/cholesteryl ester storage disease: efficacy of plant-produced human lysosomal acid lipase in mice. J Lipid Res. 2008; 49:1646–1657. [PubMed: 18413899]

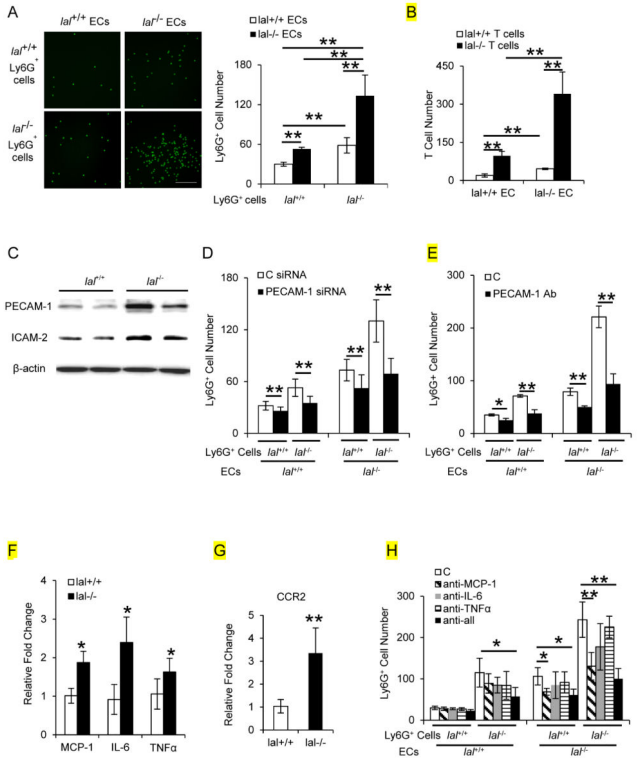

Figure 1. LAL deficiency in ECs leads to increased transendothelial migration of Ly6G$^+$ cells

(A) Transwell assay was performed to determine Ly6G$^+$ cells transmigration across the endothelial monolayer formed by *lal*$^{+/+}$ or *lal*$^{-/-}$ ECs. Six hours after seeding Ly6G$^+$ cells on the EC monolayer, the number of Ly6G$^+$ cells that have migrated to the lower chamber was counted. Bars represent 250 μm. (B) CD4$^+$ T cell transmigration across the endothelial monolayer formed by *lal*$^{+/+}$ or *lal*$^{-/-}$ ECs was examined. Six hours later, the number of transmigrating CD4$^+$ T cells was counted. (C) Expressions of PECAM-1 and ICAM-2 in ECs were determined by Western blot analysis. β-actin was used as control. Representative blots of 4 individual experiments were shown. (D) Transwell assay was performed to determine Ly6G$^+$ cells transmigration across the ECs that were transfected with PECAM-1 siRNA; (E) Transwell assay was performed to determine Ly6G$^+$ cells transmigration across the ECs that were pre-treated with anti-PECAM-1 neutralizing antibodies or control IgG; (F) Real-time PCR analysis of mRNA expression levels of MCP-1, IL-6 and TNFα in *lal*$^{+/+}$ vs. *lal*$^{-/-}$ ECs. The relative gene expression was normalized to GAPDH mRNA, and analysis was performed by the $2^{-\Delta\Delta CT}$ method. (G) Real-time PCR analysis of mRNA expression level of CCR2 in *lal*$^{+/+}$ vs. *lal*$^{-/-}$ Ly6G$^+$ cells. The relative gene expression was normalized to GAPDH mRNA, and analysis was performed by the $2^{-\Delta\Delta CT}$ method. (H) To block chemokines and cytokines, ECs were pre-treated with 10 μg/mL neutralizing antibody against MCP-1, IL-6, TNF-α individually or in combination, or control IgG for 1 h. Six hours after seeding Ly6G$^+$ cells on the EC monolayer, the number of migrating Ly6G$^+$ cells was counted. In all above experiments, data were expressed as mean ± SD; n = 4. *P < 0.05, **P < 0.01.

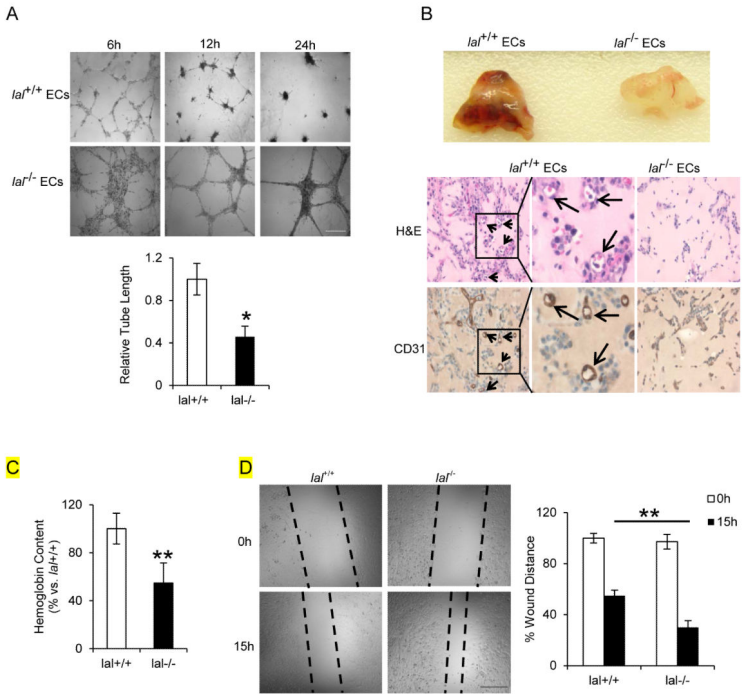

Figure 2. LAL deficiency influences EC angiogenic functions

(A) *In vitro* matrigel tube formation was performed to compare the tube-forming capability between $lal^{+/+}$ and $lal^{-/-}$ ECs. Top: representative micrographs of matrigel tube formation in ECs from $lal^{+/+}$ and $lal^{-/-}$ mice at different time interval. Bottom: statistical analysis of cumulative tube lengths at 6 h. Data were normalized to $lal^{+/+}$ ECs and expressed as mean ±SD; n = 4. *P < 0.05. (B) *In vivo* angiogenesis was assessed by matrigel plug assay. Matrigel plugs containing ECs isolated from lungs of $lal^{+/+}$ or $lal^{-/-}$ mice were implanted into $lal^{+/+}$ mice. Plugs were harvested for H&E and immunohistochemical staining 10 d after implanting *in vivo*. Representative microphotographs of matrigel plug sections stained with H&E and CD31 antibody were shown. Original magnification ×400. (C) Perfusion of matrigel plugs was determined by measuring the hemoglobin content. Data were normalized to $lal^{+/+}$ ECs and expressed as mean ±SD; n = 4, **P < 0.01; (D) The *in vitro* wound healing assay was conducted to determine EC migration in the presence of mitomycin C. Left: Representative pictures of wound healing assay of ECs from $lal^{+/+}$ or $lal^{-/-}$ mice at the beginning and end of incubation (0 and 15h, respectively). The dotted lines define the areas lacking cells. Right: Quantification of distance from one end to the other end of the wound area. Data were normalized to $lal^{+/+}$ ECs at 0 h and expressed as mean ±SD; n = 4. *P < 0.05, **P < 0.01. Bars represent 500 μm.

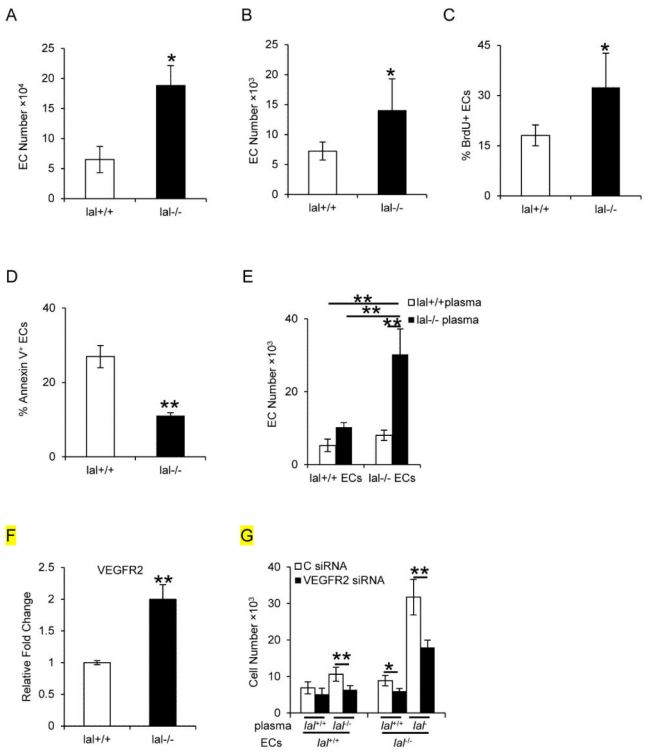

Figure 3. LAL deficiency facilitates EC proliferation

(A) Comparison of the number of $CD31^+$ cells in the lungs of $lal^{+/+}$ or $lal^{-/-}$ mice. Lung cells from $lal^{+/+}$ or $lal^{-/-}$ mice were purified by anti-CD31 microbeads and counted. (B) ECs after 3 days' culture were harvested, and the number was compared between $lal^{+/+}$ and $lal^{-/-}$ mice. (C) The percentage of BrdU incorporation into $lal^{+/+}$ or $lal^{-/-}$ ECs were analyzed by flow cytometry. (D) The percentage of Annexin V positive cells in lung $CD31^+$ cells from $lal^{+/+}$ or $lal^{-/-}$ mice. (E) ECs were cultured in medium containing 20% plasma from $lal^{+/+}$ or $lal^{-/-}$ mice for 72 h, and the cell number was counted afterwards. (F) Flow cytometry analysis of VEGFR2 expression in $lal^{+/+}$ vs. $lal^{-/-}$ ECs. Data were normalized to $lal^{+/+}$ ECs. (G) ECs transfected with VEGFR2 or control siRNA were cultured in medium containing 20% plasma from $lal^{+/+}$ or $lal^{-/-}$ mice for 72 h, and the cell number was counted afterwards. In all above experiments, data were expressed as mean ± SD; n = 3-4. *P < 0.05, **P < 0.01.

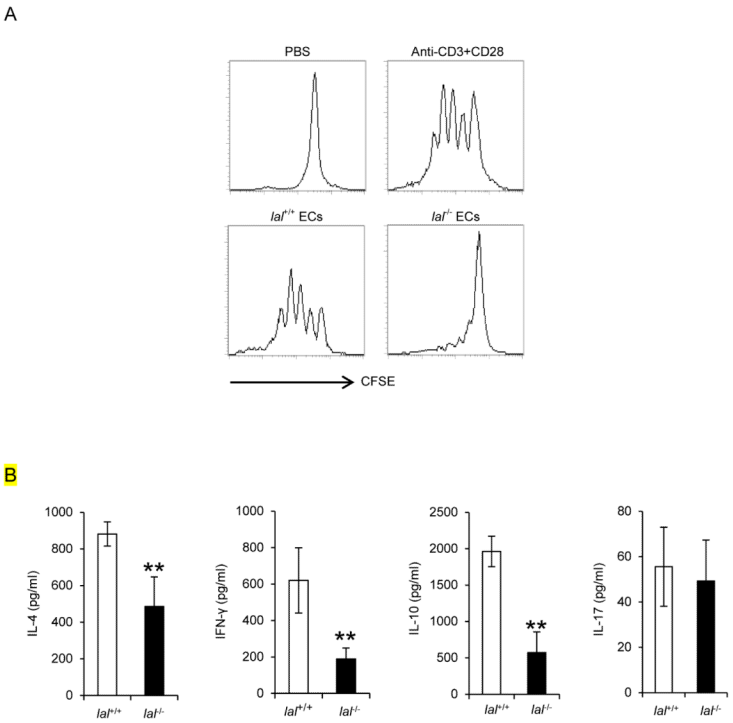

Figure 4. ECs from *lal*$^{-/-}$ mice suppress T cell proliferation and function

(A) CFSE-labeled *lal*$^{+/+}$ CD4^{+} T cells were stimulated with anti-CD3 mAb plus anti-CD28 mAb for 4 days in the presence or absence of ECs from the lungs of *lal*$^{+/+}$ or *lal*$^{-/-}$ mice at 10:1 ratio between CD4^{+} T cells: ECs. The proliferation of labeled CD4^{+} T cells was analyzed by flow cytometry. Peaks represent cell division cycles. PBS was used as a negative control. (B) The secretions of IL-4, IFN-γ, IL-10, and IL-17 of CD4^{+} T cells in the culture medium were measured by ELISA analysis. Data were expressed as mean ± SD; n = 3~4. **P < 0.01.

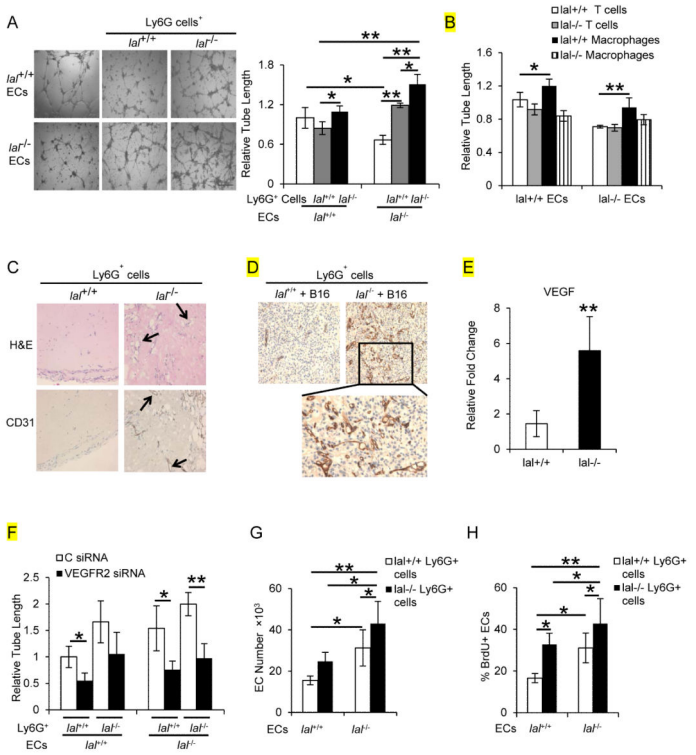

Figure 5. Ly6G$^+$ cells from *lal*$^{-/-}$ mice influence EC functions

(A) The effect of Ly6G$^+$ cells on EC tube-forming capability was determined by matrigel tube formation assay. Left: representative micrographs of tube formation in ECs co-cultured with *lal*$^{+/+}$ or *lal*$^{-/-}$ Ly6G$^+$ cells. Right: statistical analysis of cumulative tube lengths. Data were normalized to *lal*$^{+/+}$ ECs only. Bars represent 500 μm. (B) The effects of macrophages (F4/80$^+$ and CD11b$^+$) and CD4$^+$ T cells on EC tube-forming capability were determined by matrigel tube formation assay. (C) The effect of Ly6G$^+$ cells on angiogenesis in the *in vivo* matrigel plug assay. Matrigel plugs containing Ly6G$^+$ cells isolated from bone marrow of *lal*$^{+/+}$ or *lal*$^{-/-}$ mice were implanted into *lal*$^{+/+}$ mice. Plugs were harvested 14 d after implantation and analyzed by H&E and immunohistochemical staining. Representative microphotographs of matrigel plug sections stained with H&E and CD31 antibody were shown. Original magnification ×200. (D) The effect of Ly6G$^+$ cells on angiogenesis in the B16 melanoma tumor model. Matrigel mixed with B16 melanoma cells (1× 10^5) and *lal*$^{+/+}$ or *lal*$^{-/-}$ Ly6G$^+$ cells (1× 10^6) was implanted subcutaneously into *lal*$^{+/+}$ mice for 10 days. Representative microphotographs of matrigel plug sections stained with CD31 antibody were shown. Original magnification ×200. n=10. (E) Real-time PCR analysis of the mRNA expression level of VEGF in *lal*$^{+/+}$ vs. *lal*$^{-/-}$ Ly6G$^+$ cells. The relative gene expression was normalized to GAPDH mRNA, and determined by the $2^{-\Delta\Delta CT}$. (F) ECs were transfected with VEGFR2 or control siRNA, and then the effect of Ly6G$^+$ cells on EC tube-forming capability was determined by matrigel tube formation assay. Statistical analysis of cumulative tube lengths was shown. Data were normalized to *lal*$^{+/+}$ ECs only. (G) ECs after 3 days' co-culture with *lal*$^{+/+}$ or *lal*$^{-/-}$ Ly6G$^+$ cells were harvested, and the number was counted. (H) The percentage of BrdU incorporation into *lal*$^{+/+}$ or *lal*$^{-/-}$ ECs co-cultured with

$Ly6G^+$ cells was analyzed by flow cytometry. In above experiments, data were expressed as mean ± SD; n = 3-4. *P < 0.05, **P < 0.01.

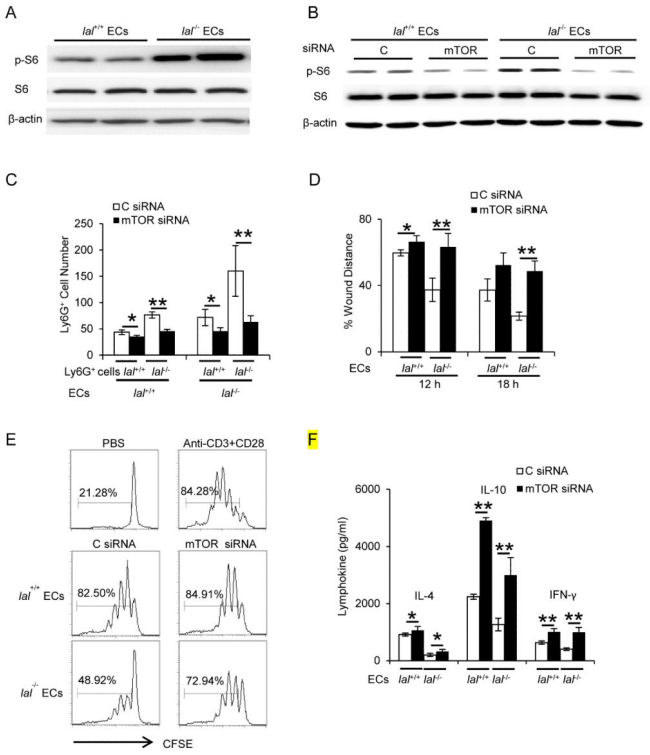

Figure 6. Activation of the mTOR pathway is involved in EC dysfunctions

(A) Expressions of phosphorylated-S6 and S6 in $lal^{+/+}$ or $lal^{-/-}$ ECs were determined by Western blot analysis. Representative blots of 4 individual experiments were shown. (B) After inhibition of mTOR in ECs by siRNA transfection, the expressions of phosphorylated-S6 and S6 were examined afterwards. Representative blots of 3 individual experiments were shown. (C) $Ly6G^+$ cells transmigration was determined after mTOR knockdown by siRNA transfection in ECs. Data were normalized to $lal^{+/+}$ $Ly6G^+$ cells transmigrating across $lal^{+/+}$ ECs with control siRNA (C siRNA) transfection and expressed as mean ± SD; n = 4-5. *P < 0.05, **P < 0.01. (D) EC migration after mTOR knockdown was assessed by *in vitro* wound healing assay in the presence of mitomycin C. Data were normalized to $lal^{+/+}$ ECs with control siRNA transfection at 0 h and expressed as mean ± SD; n = 3. *P < 0.05, **P < 0.01. Bars represent 250 μm (C) and 500 μm (D). (E) Proliferation of CFSE-labeled $lal^{+/+}$ $CD4^+$ T cells in the presence or absence of $lal^{+/+}$ or $lal^{-/-}$ ECs with mTOR or control siRNA transfection was analyzed by flow cytometry. (F) The secretion of IL-4, IL-10 and IFN-γ of $CD4^+$ T cells in the culture medium was measured by ELISA analysis. Data were expressed as mean ± SD; n = 4. *P < 0.05, **P < 0.01.

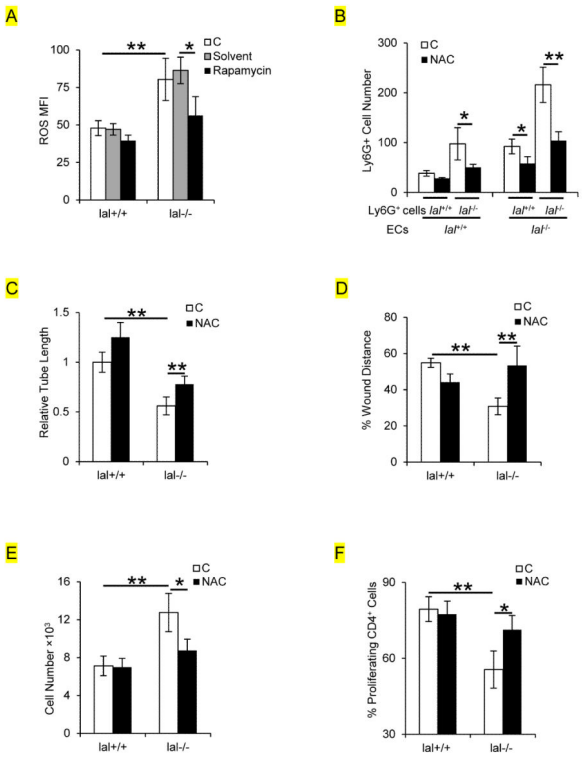

Figure 7. ROS over-production causes EC dysfunctions

(A) ROS production was increased in *lal*$^{-/-}$ ECs, which was reversed by mTOR inhibitor rapamycin. Statistical analysis of mean fluorescent intensity (MFI) of the ROS level by flow cytometry is shown. (B) Ly6G^{+} cell transmigration was determined after antioxidant NAC pre-treatment of ECs. (C) Tube formation of ECs after NAC pre-treatment. Data were normalized to *lal*$^{+/+}$ ECs. (D) EC migration after NAC treatment by *in vitro* wound healing assay at 15h in the presence of mitomycin C. Data were normalized to *lal*$^{+/+}$ ECs at 0 h. (E) EC proliferation after NAC treatment. (F) The proliferation of *lal*$^{+/+}$ CD4^{+} T cells in the presence of *lal*$^{+/+}$ or *lal*$^{-/-}$ ECs with or without NAC pre-treatment was analyzed by flow cytometry. In all above experiments, data were expressed as mean ± SD; n = 4. *P < 0.05, **P < 0.01.